Defining the Role of Arginine 96 in Green Fluorescent Protein Fluorophore Biosynthesis[†,‡]

Timothy I. Wood, David P. Barondeau, Chiharu Hitomi, Carey J. Kassmann, John A. Tainer, and Elizabeth D. Getzoff*

Department of Molecular Biology, The Skaggs Institute for Chemical Biology, The Scripps Research Institute, 10550 North Torrey Pines Road, La Jolla, California 92037

Received July 15, 2005; Revised Manuscript Received September 30, 2005

ABSTRACT: *Aequoria victoria* green fluorescent protein (GFP) is a revolutionary molecular biology tool because of its spontaneous peptide backbone cyclization and chromophore formation from residues Ser65, Tyr66, and Gly67. Here we use structure-based design, comprehensive targeted mutagenesis, and high-resolution crystallography to probe the significant functional role of conserved Arg96 (R96) in chromophore maturation. The R96M GFP variant, in which the R96M side chain is similar in volume but lacks the R96 positive charge, exhibits dramatically slower chromophore maturation kinetics (from hours to months). Comparison of the precyclized conformation of the chromophore-forming residues with the mature R96M chromophore reveals a similar Y66 conformer, contrary to the large Y66 conformational change previously defined in the slowly maturing R96A variant [Barondeau, D. P., Putnam, C. D., Kassmann, C. J., Tainer, J. A., and Getzoff, E. D. (2003) *Proc. Natl. Acad. Sci. U.S.A. 100*, 12111−12116]. Comprehensive R96 mutagenesis and fluorescent colony screening indicate that only the R96K substitution restores wild-type maturation kinetics. Further, we show that the slowly maturing R96A variant can be complemented with a Q183R second-site mutation designed to restore the missing R96 positive charge and rapid fluorophore biosynthesis. Moreover, comparative structural analysis of R96M, R96K, R96A/Q183R, and wild-type GFP reveals the importance of the presence of positive charge, rather than its exact position. Together, these structural, mutational, and biochemical results establish a pivotal role for the R96 positive charge in accelerating the GFP post-translational modification, with implications for peptide backbone cyclization in GFP, its homologues, and related biological systems.

The fluorescent chromophore of GFP[1] from *Aequoria victoria* is generated by peptide backbone cyclization of residues S65, Y66, and G67 to form a five-membered ring, followed by dehydration and oxidation reactions that conjugate the resulting imidazolone ring with the Y66 *p*-hydroxyphenyl ring (*1*−*3*; see Figure 1). The chromophore is synthesized on a distorted α-helix buried within an 11-stranded *β*-barrel (see Figure 2), which protects the fluorophore from diffusional quenchers (*2*, *4*). The chromophore's tunable spectral properties have allowed GFP to be utilized as a biosensor for determining pH and metal and halide concentrations, and as a reporter for gene expression and protein trafficking (*5*−*9*). Post-translational cyclization of the peptide backbone is not unique to GFP; it has also been observed in the formation of the imidazolone active site of histidine ammonia lyase and phenylalanine ammonia lyase (*10*−*12*), as well as in GFP homologues such as the tetrameric red fluorescent protein (RFP), which generates a GFP-like chromophore that undergoes a further oxidation reaction (*13*−*17*).

These fluorescent proteins have become vital tools in molecular and cellular research, because of their useful spectral properties and their ability to undergo spontaneous chromophore biosynthesis, in vitro and in vivo, without the need for additional cofactors, chaperones, or enzymes. GFP and RFP variants have been both designed and selected for improved spectral properties (*18*, *19*). For example, the S65T mutation improves the fluorescence quantum yield relative to that of wild-type GFP and has enhanced the signal strength for use in quantitative studies of cellular expression and trafficking (*20*). The construction of a monomeric RFP and subsequent mutagenesis produced spectral properties greatly expanding the potential range of useful wavelengths available for assessing complex interactions using fluorescence resonance energy transfer techniques (*18*). The chromophore's

[†] This work was supported by the La Jolla Interfaces in Sciences (D.P.B.), NIH Postdoctoral Fellowship GM19290 (D.P.B.), and NIH Grant RO1 GM37684 (E.D.G.). T.I.W. and D.P.B. were supported in part by The Skaggs Institute of Chemical Biology. Portions of this research were carried out at the Stanford Synchrotron Radiation Laboratory (SSRL), a national user facility operated by Stanford University on behalf of the U.S. Department of Energy, Office of Basic Energy Sciences. The SSRL Structural Molecular Biology Program is supported by the Department of Energy, Office of Biological and Environmental Research, and by the National Institutes of Health, National Center for Research Resources, Biomedical Technology Program, and the National Institute of General Medical Sciences.

[‡] Coordinates and structure factors for all reported data sets have been deposited in the Protein Data Bank as entries 2AWJ, 2AWK, 2AWL, and 2AWM.

* To whom correspondence should be addressed. Telephone: (858) 784-2878. Fax: (858) 784-2289. E-mail: edg@scripps.edu.

[1] Abbreviations: GFP, green fluorescent protein; GFPsol, GFP with solubility-enhancing mutations F64L, S65T, F99S, M153T, and V163A; HAL, histidine ammonia lyase; RFP, red fluorescent protein; PDB, Protein Data Bank; rmsd, root-mean-square deviation.

10.1021/bi051388j CCC: $30.25
Published on Web 11/17/2005

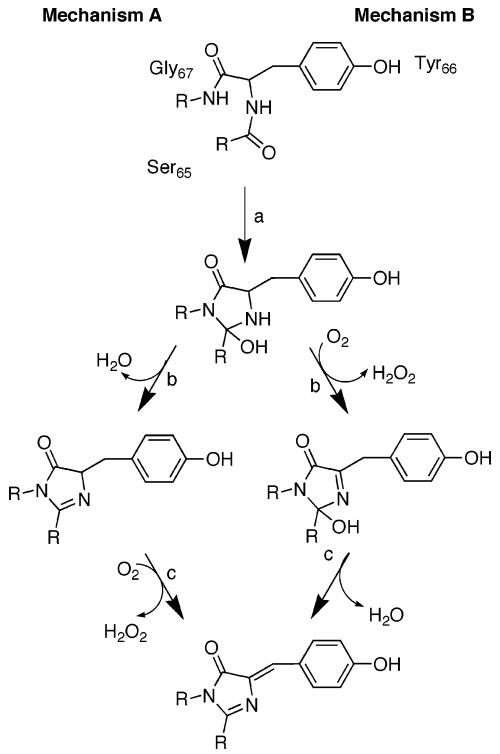

FIGURE 1: GFP chromophore maturation mechanisms. The initial ring cyclization (a) is followed by dehydration and oxidation reactions (b and c). The reaction order of dehydration and oxidation differs between mechanism A shown on the left (dehydration followed by oxidation) and mechanism B shown on the right (oxidation followed by dehydration).

spectral properties are also affected by mutations in residues outside the chromophore, such as T203Y, which is responsible for the spectral shift of yellow fluorescent protein (*21*). The protein environment is key to fluorophore tuning, biosynthesis, and maturation, yet the identities and roles of the residues contributing to these functions remain poorly understood.

Recently determined structures for GFP variants R96A and S65G/Y66G captured before, as well as after, peptide backbone cyclization provided insights into the driving force for spontaneous fluorophore biosynthesis in GFP (*22*). A dramatic bend in the central helix forces the G67 nitrogen atom into van der Waals contact with the carbonyl oxygen atom at position 65 in preparation for covalent bond formation, and also eliminates potential helical hydrogen bonds that would otherwise have to be broken at an energetic cost during peptide cyclization (*22*, *23*). In structures of wild-type GFP (see Figure 2) and of both the pre- and postcyclized forms of the S65G/Y66G variant, the side chain of R96 stretches inward from the β-barrel toward the chromophore on the convex side of the bent central helix. The R96 guanidinium group forms hydrogen bonds with the T62 and Y66 carbonyl oxygen atoms freed at the helix bend. In the absence of R96, the precyclized R96A variant forms additional main chain helical hydrogen bonds (α-helical T62−Y66 and 3_{10}-helical S65T−V68) that are not found in the mature R96A structure, and therefore must be broken for cyclization (*22*). Also, the side chain of central chromophore-forming residue Y66 has rotated nearly 180° from its position in the mature chromophore and into a cavity created by the R96A truncation. Interestingly, truncation of R96 by the R96A mutation also slowed chromophore maturation ~1000-fold from the hours estimated for wild-type GFP (*3*, *24*) to months (*22*). This arginine is conserved in all GFP-like proteins, yet its precise role in chromophore biosynthesis has remained elusive.

Three different features of the R96 side chain could be critical to rapid chromophore formation in GFP: steric properties, hydrogen bonding, and positive charge. R96 may sterically promote chromophore formation by preorganizing the Y66 side chain and flanking main chain, as suggested by the structural comparisons (*22*) described above for GFP variants before and after ring formation. The R96 hydrogen bond with the Y66 carbonyl oxygen (becomes the O2

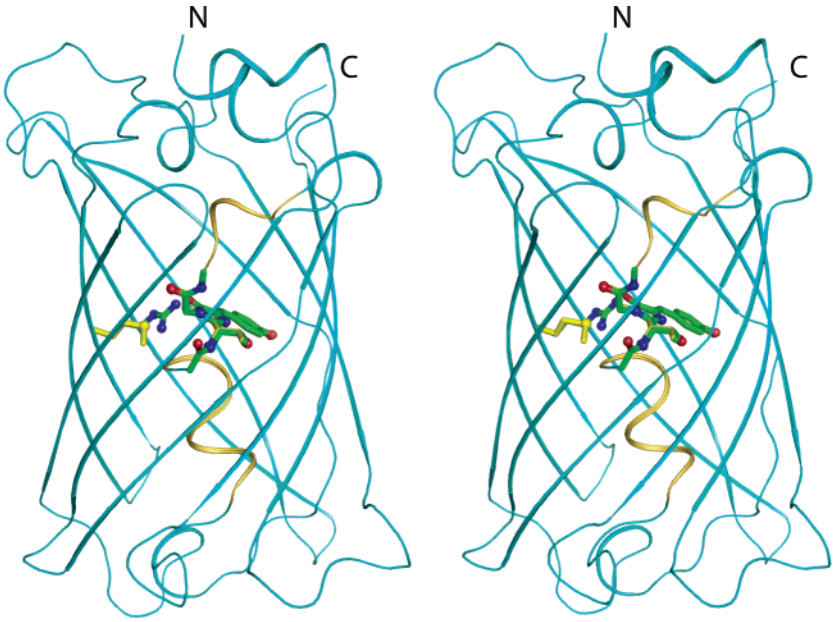

FIGURE 2: GFP fold and chromophore environment. The GFP β-barrel fold (cyan) surrounds a bent central helix (gold) containing the chromophore-forming residues (green), and shields the chromophore from bulk solvent, increasing fluorescent yield. Wild-type R96 (green) and mutant R96M (yellow) side chains face toward the interior of the barrel. R96 buries its positive charge near the chromophore and hydrogen bonds to the imidazolone oxygen atom. The protein N-terminus and C-terminus are labeled N and C, respectively.

Table 1: Crystallographic Data Collection and Refinement Statistics[a]

	precyclized R96M	mature R96M	mature R96K	mature R96A/Q183R
beamline (at SSRL)	7-1	9-1	9-1	9-1
wavelength (Å)	1.08	0.979	0.979	0.984
unit cell parameters				
a (Å)	51.20	51.24	51.09	51.51
b (Å)	62.77	62.35	62.42	62.34
c (Å)	71.43	71.07	71.52	71.26
resolution range (Å)	20−1.6 (1.66−1.6)	20−1.15 (1.19−1.15)	20−1.85 (1.92−1.85)	50−1.70 (1.76−1.70)
no. of total/unique observations	114672/30130	217613/74907	61189/19979	66674/24741
completeness (%)	96.9 (95.0)	91.9 (67.1)	99.0 (99.3)	95.3 (91.2)
R_{sym} (%)[b]	8.6 (42.6)	3.7 (35.9)	9.0 (36.1)	5.7 (35.6)
$I/\sigma I$	21.60 (5.43)	26.06 (2.39)	12.03 (3.78)	18.42 (3.42)
no. of refinement parameters	8309	19290	8476	8463
R_{work} (%), R_{free} (%)[c]	18.50, 24.08	14.85, 19.98	21.16, 27.00	16.43, 22.32
average Wilson *B*-factor (Å^2)	17.3	8.9	6.0	10.9
rms deviations from ideal values				
bond lengths (Å)	0.008	0.014	0.01	0.007
1−3 bond distances (Å)[d]	0.025	0.031	1.6	0.023
PDB entry	2AWJ	2AWK	2AWL	2AWM

[a] All crystals belong to the $P2_12_12_1$ space group. Values in parentheses are the statistics for the highest-resolution shell of data. [b] $R_{sym} = \sum[I_{hkl} - (I)]/\sum(I)$, where I is the average individual measurement of I_{hkl}. [c] $R_{work} = (\sum|F_{obs} - F_{calc}|)/\sum|F_{obs}|$, where F_{obs} and F_{calc} are the observed and calculated structure factors, respectively. [d] For the R96K structure, the bond angle rmsd is given in degrees (refined in CNS). All other structures were refined using SHELX97.

carbonyl of the five-membered imidazolone ring of the chromophore) may promote cyclization by facilitating deprotonation of the G67 backbone nitrogen for nucleophilic attack of the S65 carbonyl (see Figure 1). Thus, R96 may function as a main chain hydrogen bond donor that inhibits alternative, nonproductive, backbone conformations (a negative design feature) and/or activates ring formation (a positive design feature) (*25*). Last, R96 buries a positive charge near both the precyclized amino acids and the mature chromophore. All of these R96 features differ between the R96A and wild-type proteins, and individually or in combination may serve to explain the dramatically slowed chromophore formation kinetics in the R96A variant.

To better define how R96 accelerates chromophore formation, we spectroscopically and structurally characterized site-directed mutants designed to separate and test these potential roles for R96 in chromophore maturation. In the R96M variant, the methionine substitution mimics the steric constraints but not the hydrogen bonds or positive charge of the wild-type arginine, yet this variant exhibits very slow chromophore maturation. Comprehensive R96 mutagenesis coupled to a colony screening methodology revealed that only lysine and wild-type arginine support rapid fluorophore formation. Moreover, reengineering a positive charge into the R96A variant through a second-site mutation restored rapid maturation kinetics. Together, these results indicate a primary electrostatic role for R96 in the class of fluorescent proteins, which we discuss in terms of the chemical steps of GFP fluorophore biosynthesis.

EXPERIMENTAL PROCEDURES

Mutant Cloning, Protein Purification, and Site-Directed Random Mutagenesis. Site-specific GFP variants were generated by the Quikchange method (Stratagene) using a pET11a-derived vector encoding a solubility-optimized GFP [GFPsol or GFP with the F64L, S65T, F99S, M153T, and V163A mutations (*26*, *34*, *35*)] gene under transcription control of the T7 promoter (pDPB325). Mutants were confirmed by sequencing. Recombinant GFP proteins were expressed and purified as described previously (*8*, *22*, *27*). The plasmid encoding the R96A GFP variant [pDPB126 (*22*)] was used as a template for Quikchange mutagenesis (Stratagene), using PCR primers completely degenerate at the residue 96 position, to generate a full library of possible codons. The library was transformed into electrocompetent BL21(DE3) cells (Stratagene), and isolated colonies were obtained by selecting for ampicillin resistance on LB plates. Colonies were incubated at 37 °C overnight, and then their fluorescence phenotype was scored by observing the presence or absence of fluorescence under a hand-held UV lamp. Both fluorescent and nonfluorescent colonies were grown in liquid culture, and the plasmid DNA was isolated for sequencing.

Crystallographic Methods. GFP crystals were grown as described previously (*8*, *22*). Briefly, hanging drops containing 3 μL of protein (10 mg/mL) and 3 μL of a diluted microseed solution were used to grow crystals with mother liquor containing 10−20% PEG4000, 50 mM Hepes (pH 8.0), and 50 mM magnesium chloride. Diffraction data were collected at the Stanford Synchrotron Radiation Laboratory (SSRL) (Table 1). Data were indexed and reduced using the Denzo/Scalepack packages (*28*). Each structure was determined by molecular replacement with Amore in the CCP4 version 4.2.1 package (*29*), using wild-type GFP with the chromophore deleted as a probe. The structures were refined with iterative rounds of fitting with Xtalview (*30*) and crystallographic refinement with CNS version 1.1 (*31*). SHELX-97 (*32*) was used in later refinement rounds for diffraction data sets with 1.7 Å or better resolution.

Modeling and Figure Generation. Modeling of the R96K substitution into the R96M precyclized structure was done using the least-squares fit (whole model) function of the Xtal-View program Xfit to overlay the Cα atoms for approximation of the lysine side chain position in the precyclized state (*30*). Figures were generated using AVS (*33*).

RESULTS

Spectroscopic and Structural Characterization of the R96M Slow Maturation GFP Variant. To experimentally test

Table 2: Chromophore Excitation and Emission[a]

protein	pK_a	absorbance peaks (nm)		fluorescence emission (390 nm excitation)	
		P	*D*	peak A	peak B
R96M	7.9 ± 0.3	383	466	449	490
R96K	6.8 ± 0.2	383	473	450	509
R96A/Q183R	5.8 ± 0.3	384	489	450	510
GFPsol	5.9 ± 0.1	383/396	489	450	505

[a] *P* [absorbance peak (nanometers) assigned to protonated species], *D* [absorbance peak (nanometers) assigned to deprotonated species], and peaks A (minor peak) and B (major peak) represent fluorescence peaks upon excitation with light.

and distinguish the possible roles for residue R96 in the mechanism of GFP chromophore formation (Figure 1) within the protein environment (Figure 2), we designed site-directed mutants, determined their crystallographic structures (Table 1), and analyzed them spectroscopically (Table 2). To examine the effect of a long but uncharged side chain at position 96, we introduced the R96M mutation into GFPsol [GFP with solubility-enhancing mutations F64L, S65T, F99S, M153T, and V163A (*26*, *34*, *35*)]. When initially purified, the R96M protein was colorless. The visible absorbance characteristic of the mature chromophore only appeared after a 2 month (~1500 h) incubation at 37 °C [in 50 mM Hepes buffer (pH 8.0)]. R96M therefore has very slow maturation kinetics, similar to those of the R96A variant (*22*).

The matured R96M protein exhibited a pH-dependent UV−visible absorbance spectrum with a major absorbance maximum at 466 nm and a secondary peak at 383 nm (Table 2). Incubation of R96M at different pH values revealed that the protonated species absorbing at 383 nm was reversibly interconverted to the deprotonated species absorbing at 466 nm, with an isosbestic point indicating a pK_a of 7.9 ± 0.3. The fluorescence emission maximum for the R96M protein was at 490 nm (Table 2). Thus, the R96M spectroscopic properties were reminiscent of those of wild-type GFP [489 and 396 nm absorbance maxima and fluorescence emission at 505 nm (*6*)], but more similar to those of the R96A (*22*) and R96C (*36*) variants, reported with absorbance maxima at 468 nm and fluorescence emission at 503 nm. Interestingly, in addition to the blue-shifted absorbance properties, the R96M substitution resulted in a pK_a shift of the chromophore from 5.9 ± 0.1 in GFPsol (*6*) to 7.9 ± 0.3 (Table 2).

To assess the molecular details of the chromophore environment that led to these altered spectroscopic properties, we determined a 1.15 Å resolution crystallographic structure of the mature fluorescent R96M variant (Table 1). The structures of the mature R96M variant and its GFPsol parent are nearly identical: the bent central helix with breaks in the main chain helical hydrogen bonding (*22*) is conserved (Figure 2), and differences are limited to very minor side chain conformational changes near the mutation site (Figure 3A). The mutated R96M side chain conformation follows that of wild-type R96 through the Cγ atom, with the Sδ and terminal methyl moieties overlaying the R96 guanidinium group. In the R96M variant, the chromophore O2 atom maintained two hydrogen-bonding partners: the Q94 side chain, as in wild-type GFP (*2*, *4*), and a solvent water molecule replaced wild-type R96. Thus, the primary difference in the immediate chromophore environment between the R96M and GFPsol proteins is the positive charge lost due to the R96M substitution.

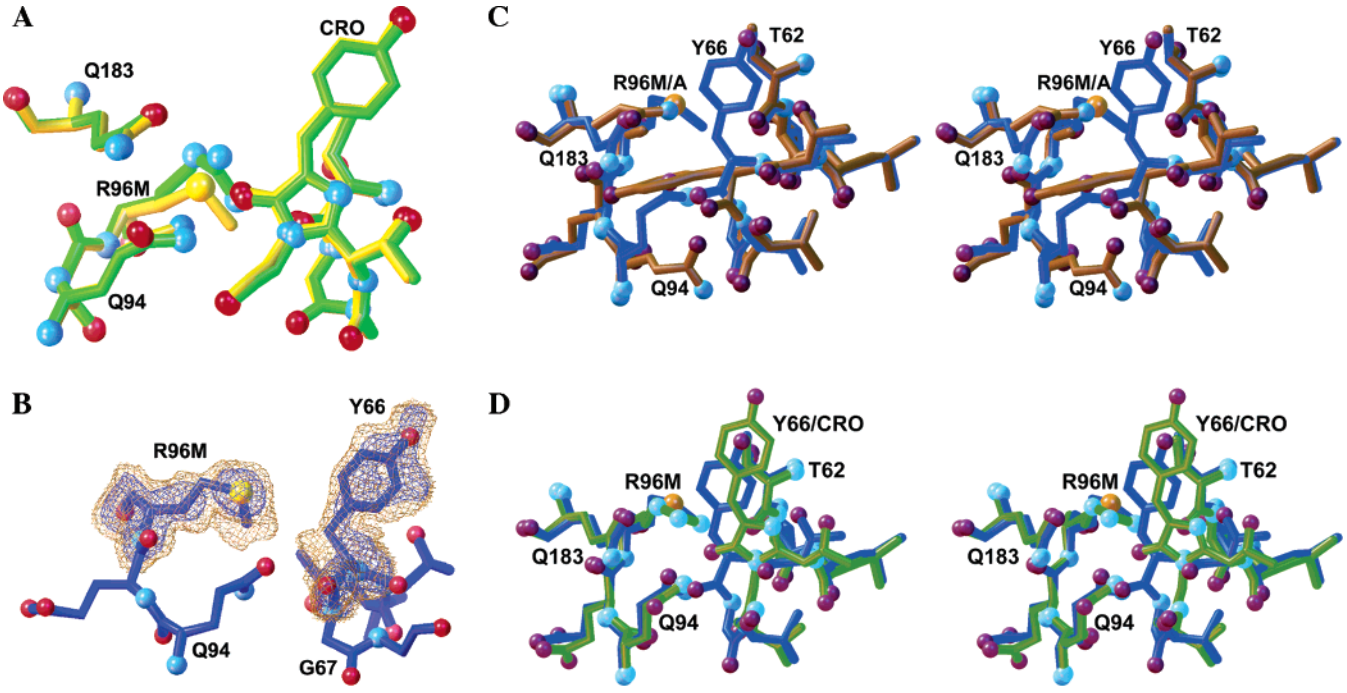

FIGURE 3: Structural analysis of the slowly maturing R96M GFP variant. (A) Superposition of mature R96M variant (yellow) and wild-type GFP (green) structures, showing identical chromophores (CRO) and similar conformations for the mutated R96M (yellow) and wild-type R96 (green) side chains. (B) Precyclized chromophore residues and nearby R96M shown with omit map density, contoured at 1σ (gold) and 3σ (blue), from the R96M precyclized structure. The contoured density indicates a small population of additional chromophore conformation(s) exist within the crystal, but the mature chromophore species does not fit the additional density. (C) Superposition of structures for precyclized R96M (blue) and precyclized R96A (gold) variants showing different conformers for Y66, but a similar backbone shift of the chromophore-forming residues toward the cavity generated by the R96 mutations. (D) Superposition of structures for the precyclized R96M (blue) variant and mature wild-type GFP (green), highlighting the backbone atom shift of the chromophore-forming residues found in the mutants lacking R96.

The slowed chromophore maturation kinetics of the R96M variant allowed for structural interrogation of the protein in the precursor as well as the mature fluorophore states. We therefore purified and crystallized the colorless R96M protein and determined the crystallographic structure to 1.60 Å resolution (Table 1). Difference and omit electron density maps revealed a predominantly precyclized conformation for the chromophore-forming residues (Figure 3B). The precyclized structures of R96M and R96A superimpose well (Figure 3C), exhibiting an overall Cα rmsd of 0.23 Å. The only significant differences are the increased length of the R96M side chain, the movement of Q94 imposed by the Y66 side chain position, and the different conformation of the central chromophore-forming residue Y66. The Y66 side chain of the R96M variant, unlike that of the R96A variant (*22*), adopted a Cα−Cβ vector and χ1 torsion similar to that of Y66 in wild-type GFP (*2*, *4*) and occupied much of the same volume. Comparison of the pre- and postcyclized R96M structures (Figure 3D) showed that the chromophore-forming residues are not preorganized for cyclization. Instead, before cyclization, central chromophore residue Y66 and the flanking backbone are shifted (∼2 Å) toward the shorter mutated side chain at position 96 (Figure 3D), and two additional helical hydrogen bonds [T62−Y66 (α-helix) and S65T−V68 (3_{10}-helix)] are created, as in the R96A side chain truncation variant (*22*). Thus, these slow maturation mutants both exhibit additional hydrogen bonds to preferentially stabilize the chromophore-forming residues in their precyclized state.

Comprehensive Mutagenesis of R96 and Screening for Chromophore Formation. To further explore which features of R96 participate in chromophore maturation, we developed an agar plate assay for GFP fluorescence and probed all possible R96 substitutions for rapid fluorophore biosynthesis. The comprehensive random mutagenesis and colony-based fluorescence assay revealed that only colonies expressing wild-type R96 GFP or the R96K variant synthesized fluorophores rapidly (defined as overnight expression of fluorescent protein comparable to that of wild-type GFP expressed under similar conditions). The residue 96 codon was randomized in the R96A expression vector by using degenerate oligonucleotides. The resultant library (>5000 isolates) was screened for the ability to recover fluorescent bacterial colonies; all fluorescent colonies and >150 nonfluorescent colonies were sequenced. Multiple codons for either the positively charged R96 or R96K substitution gave rise to fluorescent colonies (Table 3, less than 1% of library isolates). All other amino acid substitutions at position 96 produced nonfluorescent colonies (Figure 2 of the Supporting Information), indicating that these mutant proteins were poorly expressed, did not fold, or did not rapidly form chromophores. Our primary concern in this experiment was obtaining a complete 20-amino acid set of GFP variants at position 96, to test if any residues other than arginine would recover rapid fluorescence maturation. This complete set was obtained by using site-directed mutagenesis to generate missing variants (Table 3), but no additional recovery mutants were found. Subsequent expression of the nonfluorescent mutants in liquid culture confirmed expression levels of GFP protein comparable to those found in the fluorescent colonies (data not shown). The rapid chromophore maturation kinetics of the R96K variant led us to purify and structurally characterize this protein.

Table 3: Rapid Fluorescence Recovery[a]

residue	fluorescence	codon recovered
Ala	−	GCA, GCC, GCG
Arg	***	AGA, AGG, CGT
Asn	−	AAC (oligo)
Asp	−	GAC (oligo)
Cys	−	TGT
Gln	−	CAA (oligo)
Glu	−	GAA
Gly	−	GGC, GGG
His	−	CAT
Ile	−	ATA (oligo)
Leu	−	CTT, TTG
Lys	***	AAA, AAG
Met	−	ATG
Phe	−	TTT
Pro	−	CCA (oligo)
Ser	−	TCC, AGC
Thr	−	ACT
Trp	−	TGG (oligo)
Tyr	−	TAC (oligo)
Val	−	GTG, GTA
stop	−	TAA, TGA

[a] Only positively charged Arg and Lys residues restore fluorescence on the wild-type time scale (denoted with three asterisks). All other substitutions yield nonfluorescent colonies (denoted with a dash). Recovered codons are listed in the third column, where (oligo) indicates a mutation was generated by site-specific mutagenesis.

Structural and Spectroscopic Characterization of the R96K Positive Charge Replacement Variant. Despite its wild-type chromophore maturation kinetics, the R96K variant exhibits an altered chromophore environment and spectroscopic properties. The R96K crystallographic structure, determined to 1.85 Å resolution (Table 1), revealed a mature chromophore with an overall conformation similar to that of wild type GFP (Figure 4A). The R96K side chain followed the wild-type R96 conformation (Figure 4A) and maintained the wild-type hydrogen bond with the T62 carbonyl oxygen (Figure 4B). However, in contrast to R96, the R96K side chain failed to form hydrogen bonds with either the chromophore O2 atom or the Q183 OE1 atom (Figure 4B). The loss of direct interactions between the R96 side chain and the chromophore explains the significantly blue-shifted absorbance maximum for the deprotonated chromophore in the R96K variant (Table 2). These spectroscopic properties indicate that stabilization of the deprotonated chromophore by the side chain of R96K (absorbance maximum of 473 nm) is intermediate between that of R96M (466 nm) and that of R96 (489 nm).

To check if the smaller and more flexible R96K side chain was likely to mimic the role of R96 in preorganizing the chromophore-forming residues for cyclization, we modeled (see Experimental Procedures) the R96K side chain conformer observed in the mature R96K structure (Figure 4A) into the precyclized R96M structure (Figure 3B−D). In this model (Figure 1 of the Supporting Information), the R96K side chain maintained the hydrogen bond to the T62 carbonyl found in the structure of the mature R96K variant, and did not introduce any significant van der Waals collisions (closest contact is 3.4 Å between the R96K Nζ and Y66 Cβ atoms) into the precyclized structure of the R96M variant (Figure 1 of the Supporting Information). This modeling suggests that in the precyclized state, the chromophore-forming residues of the R96K variant are more likely to be shifted toward the shorter R96 residue (like those in R96M, Figure 3D) than

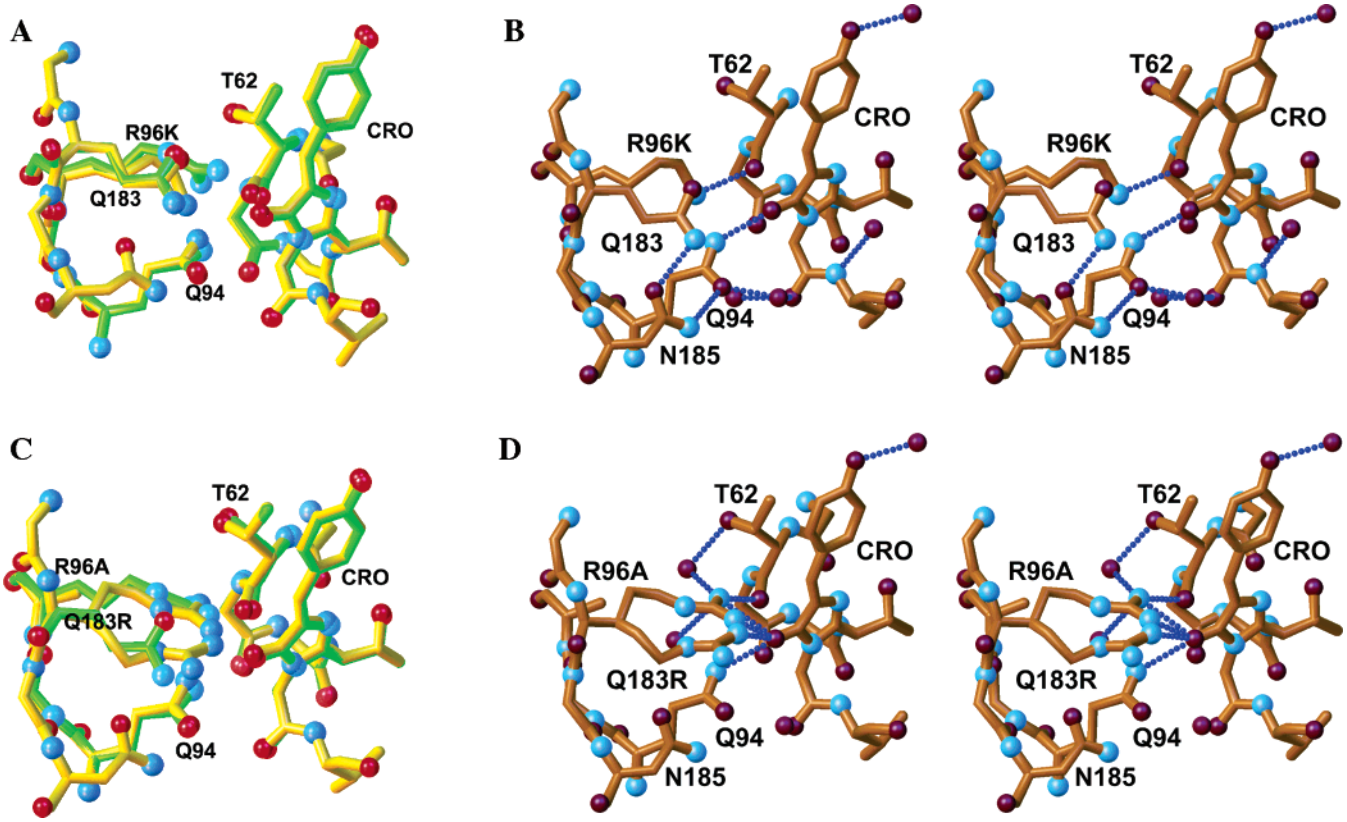

FIGURE 4: Structures of recovery mutants R96K and R96A/Q183R. (A) Overlay of R96K mutant (yellow) and wild-type GFP (green) structures, showing the identical mature chromophores, and similar conformations for the R96K (yellow) and wild-type R96 (green) side chains. (B) Stereo pairs showing the hydrogen bonding network (lines of small blue spheres) in the R96K mutant among the R96K, Q183, T62 and chromophore residues, and solvent molecules (red spheres) involved in hydrogen bond interactions for the R96K mutant. (C) Overlay of R96A/Q183R double mutant (yellow) and wild-type GFP (green) structures, showing how Q183R (dual conformers) replaces the positive charge of R96 yielding a wild-type chromophore. (D) Stereo pairs showing the hydrogen bonding network in the R96A/Q183R double mutant, with the Q183R guanidinium group forming hydrogen bonds to both the T62 carbonyl oxygen and chromophore imidazolone oxygen atoms, similar to the R96 hydrogen bonding pattern seen in the wild-type protein. Hydrogen bonds and solvent molecules are represented as in panel B. The extended length of the Q183R side chain does not allow for the hydrogen bond normally between the Q183 and N185 side chains as seen in wild-type GFP.

preorganized for chromophore formation by the full-length R96 side chain [as in the precyclized structure of the S65G/Y66G variant (*22*)]. Yet the differences in chromophore maturation kinetics between the rapidly maturing R96K and slowly maturing R96M variants are striking, suggesting that steric properties of R96 do not dominate chromophore maturation kinetics.

Double Mutant R96A/Q183R Restores Rapid Chromophore Formation Kinetics. Given the long-range, orientation-independent nature of electrostatic interactions, we reasoned that the slow maturation of the R96A mutant could be rescued by the introduction of a nearby positively charged residue. Modeling suggested that the Q183R substitution in the R96A background could restore a positive charge near the chromophore-forming residues, with fewer steric restrictions than those imposed on the wild-type R96 side chain. The designed and engineered R96A/Q183R protein exhibited rapid, wild-type, maturation kinetics, confirming our hypothesis. Moreover, the spectral properties of the purified R96A/Q183R protein are even more similar to those of wild-type GFP than are those of the R96K variant (Table 2).

To examine the chromophore environment of the reintroduced positive charge in the double mutant, we determined a 1.70 Å resolution structure for the R96A/Q183R mutant. The Q183R side chain has two conformations, one acting as a superb mimic of R96 (Figure 4D). In this R96-like conformation, hydrogen bonds from Q183R NH1 are made with the chromophore O2 oxygen atom (2.7 Å for Q183R vs 2.8 Å for the R96 NH2 atom), the T62 carbonyl (3.0 Å for Q183R vs 2.8 Å for the R96 NH1 atom), and a solvent molecule (2.4 Å for Q183R vs 2.9 Å for the R96 NH1 atom) located in the cavity generated by the R96A mutation (Figure 4D). In the second Q183R conformation, the side chain forms hydrogen bonds with the Q69 side chain oxygen and not the T62 carbonyl; however, the NH2 atom is still hydrogen bonded to the chromophore O2 oxygen atom (2.8 Å). Together, the contrasting kinetics but similar sterics of the R96M and R96K variants, the comprehensive mutagenesis results, and the R96A/Q183R recovery mutant's structure and maturation kinetics all indicate a primarily electrostatic role for R96 in chromophore formation.

DISCUSSION

GFP and its homologues undergo a remarkable post-translational modification to create fluorophores out of three component amino acids. Extensive mutagenesis of these chromophore residues and their neighbors generally alters the spectral properties of the chromophore, rather than disrupting its maturation (*3*, *24*, *37*), implicating a major role for the protein architecture in chromophore biosynthesis (*22*). Interestingly, residues adjacent to the chromophore-forming residues in the central α-helix and those that surround the

chromophore are generally not conserved in GFP homologues. R96 and E222 are two exceptions. Here we explore the functional role of R96 in GFP spectral tuning and chromophore biosynthesis.

Spectral Tuning of the Chromophore by Residue 96. Our results indicate that R96 tunes the GFP spectral properties by stabilizing the deprotonated form of the mature chromophore. The charge-neutralizing R96M substitution blue shifts the absorbance maximum for the deprotonated species (from 489 to 466 nm), as found for the R96A and R96C variants (*22*, *36*), and increases the pK_a of the chromophore from 5.9 ± 0.1 to 7.9 ± 0.3. The R96K substitution maintains a positive charge, but places it farther from the chromophore. Consequently, the R96K variant exhibits values for the absorbance maximum of the deprotonated species and the pK_a values that are intermediate between those of the wild type and R96M proteins (Table 2). The R96A/Q183R variant, which positions the positive charge similarly to wild-type R96, has spectral properties nearly identical to those of its GFPsol parent. None of these substitutions significantly alters the absorbance maximum for the protonated chromophore (Table 2). Our data suggest a positive electrostatic role for R96 in stabilizing the deprotonated form of the chromophore. This conclusion is consistent with previous studies by Wachter et al. (*38*) of the GFP T203Y variant known as yellow fluorescent protein, in which negatively charged halide ions hydrogen bond to T203Y, thereby masking the positive charge of R96 and increasing the pK_a of the chromophore from 5.2 to 7.0. Taken together, these results indicate that R96 has an electrostatic role in the spectral tuning of the mature chromophore; however, we suggest its primary function is in fluorophore biosynthesis.

Defining the Roles of R96 in Chromophore Maturation. Many different roles for R96 in fluorophore biosynthesis have been proposed: hydrogen bonds, steric constraints, and/or electrostatic interactions of R96 could each affect multiple steps of the GFP chromophore maturation pathway. First, R96 hydrogen bonding interactions may assist in chromophore formation by activating the S65 carbonyl for nucleophilic attack (*23*) or by directly deprotonating the G67 backbone amide (*39*). Second, R96 steric properties may selectively inhibit conformers of the Y66 side chain (*22*) and/or preorganize the backbone of the chromophore-forming residues to align molecular orbitals for ring cyclization (*25*). Third, R96 electrostatic interactions may both favor G67 nitrogen deprotonation and stabilize the proposed enolate intermediates (*25*) in the cyclization reaction (Figure 5). Moreover, R96 may provide an O_2 binding site and accelerate chromophore oxidation by facilitating electron transfer and superoxide formation, analogous to the electrostatic role proposed for the Cu site in amine oxidase (*40*). By combining comprehensive mutagenesis and kinetic analyses with structure and design studies, we were able to separate and test these potential roles for R96 in chromophore maturation.

Residue 96 Hydrogen Bonding Interactions Involved in Chromophore Maturation. To test if specific R96 hydrogen bonding interactions assist in chromophore formation, we determined the precursor structure of the slowly maturing R96M variant and also modeled into it the side chain R96K substitution, which restores rapid maturation. Although R96 hydrogen bonding was proposed to directly activate the S65 carbonyl for nucleophilic attack (*23*) or deprotonate the G67 backbone amide (*39*), the R96 guanidinium group does not

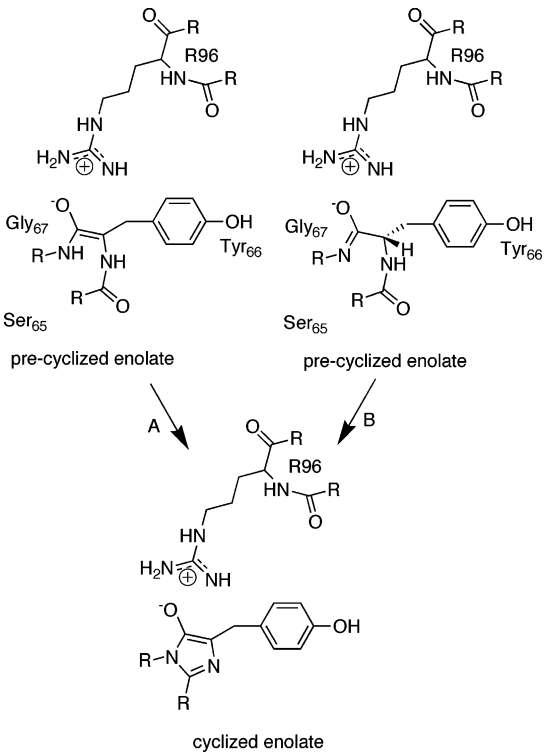

FIGURE 5: Mechanistic role for R96 electrostatics in stabilizing potential enolate intermediates. The positive charge provided by the R96 guanidinium group can stabilize the possible enolate intermediates during maturation of the GFP chromophore. The precyclized enolate tautomers can both proceed to the cyclized state as shown in parts A and B. The cyclization state need not affect the long-range interaction between R96 and the Y66 carbonyl, though we favor the interaction with the cyclized intermediate form shown at the bottom.

interact directly with either the S65 carbonyl oxygen or G67 nitrogen atoms in the precyclized structure of the S65G/Y66G variant (*22*), but instead forms hydrogen bonds with the carbonyl oxygen atoms of T62 and Y66, the Q183 side chain oxygen atom, and a water molecule. Of these, the interaction most likely to affect chromophore maturation is the hydrogen bond between the positively charged R96 side chain and the carbonyl oxygen of the chromophore-forming residue Y66, yet this hydrogen bond is not made by either the R96M or R96K variant. Here in our precyclized structure of the slowly maturing R96M variant, the Y66 carbonyl oxygen atom forms a hydrogen bond with a solvent water molecule. Modeling the R96K substitution into this precyclized structure of R96M reveals that the Nζ atom may interact with the T62 backbone carbonyl, but not with the carbonyl of Y66. Thus, residue 96 hydrogen bond interactions with the Y66 carbonyl oxygen do not correlate with rapid maturation kinetics and are not likely a critical component of the fluorophore biosynthesis mechanism.

Do R96 Steric Interactions Accelerate Chromophore Maturation? We determined and compared structures of the R96M variant in the precyclized and mature chromophore states to evaluate steric roles for R96 in accelerating chromophore maturation by preorganizing the chromophore-forming residues. On the basis of our structural analyses, R96 may sterically prevent conformations of the Y66 side chain and main chain that would stabilize the uncyclized chromophore or increase the activation energy for cyclization, thereby acting as a negative design feature.

In the previously determined precyclized structure of the R96A slow maturation variant, the Y66 side chain filled a cavity created by the R96A truncation (*22*). Thus, to form a mature chromophore, this Y66 side chain must rotate nearly 180°, with the phenolic oxygen atom moving a remarkable 14 Å between the pre- and postcyclized moieties. Here, our precyclized structure of the slowly maturing R96M variant (Figure 3) revealed that the larger methionine side chain precluded this nonfluorophore-like Y66 conformer. Thus, Y66 side chain conformer selectivity is not a critical determinant for fast maturation.

Our new results cannot completely rule out a steric role for R96 in chromophore formation. Despite exhibiting similar Y66 and R96M side chain conformations before and after chromophore formation, the precyclized R96M variant does exhibit a backbone shift of chromophore-forming residues 65−67 away from the position of the mature chromophore and toward the cavity left by the R96 truncation (Figure 3D), as was also seen for the R96A variant (*22*). In both these slowly maturing mutants, this backbone shift is accompanied by the formation of two additional helical hydrogen bonds [T62−Y66 (α-helix) and S65T−V68 (3_{10}-helix)] that must be broken to allow cyclization during chromophore formation. In contrast, the chromophore-forming backbone atoms of the precyclized, R96-containing, S65G/Y66G variant are not shifted (*22*), suggesting that the R96 may play a steric role in preventing this shift and thus promoting cyclization.

To more broadly probe the role of R96, we used comprehensive mutagenesis and fluorescent plate screening methods to show that, of the 20 naturally occurring amino acids, only Lys or Arg substitutions at position 96 restored rapid maturation kinetics to the R96A variant (Table 3, Figure 2 of the Supporting Information). In addition to retaining the positive charge of R96, the Lys substitution contains a longer side chain than Met and is better able to sterically mimic R96. Thus, the faster chromophore maturation for the R96K variant compared to the R96M variant may be due to the addition of the positive charge or to the ability of the larger side chain to sterically disfavor conformations stabilizing the precursor state. However, our model substituting R96K into the precyclized R96M structure (Figure 1 of the Supporting Information) did not produce van der Waals collisions, suggesting that the size increase from methionine to lysine was not responsible for the change in maturation kinetics. Thus, the R96 charge alone appears to be sufficient to promote rapid chromophore maturation, and potential steric roles for R96 are not critical.

Electrostatic Interactions of Residue 96 in Chromophore Maturation. Taken together, our structural and mutational results strongly support an electrostatic role for R96 in fluorophore biosynthesis. The comprehensive mutagenesis and colony scoring results indicate that only the positively charged amino acids Arg and Lys are able to promote rapid fluorophore formation. Further, we were able to recover function in the R96A variant through introduction of the second-site positively charged mutation Q183R. Structural analysis of the R96K and R96A/Q183R variants in comparison to wild-type GFP reveals that the presence, rather than the exact position, of the positively charged side chain is the critical factor for rapid chromophore maturation. This is consistent with the long-range, orientation-independent, nature of electrostatic interactions. In GFP, this positive charge of R96 may affect at least four different steps of chromophore maturation: (1) peptide backbone cyclization, (2) formation of an enolate intermediate, (3) main chain dehydration, and (4) oxidation to generate the mature chromophore. In wild-type GFP, peptide cyclization is rapid and the rate-limiting step in chromophore maturation is the oxidation reaction (*3*). The ability to isolate the R96M and R96A variants in the precyclized state suggests that the loss of positive charge may change the rate-limiting step of fluorophore synthesis from oxidation to either peptide cyclization or stabilization of the cyclized product.

We propose that the hydrogen bond from R96 to the Y66 carbonyl oxygen atom, destined to become the chromophore O2 atom, is the most likely candidate for mediating the effects of the R96 positive charge on the chromophore maturation mechanism. The R96 positive charge would complement the negatively charged Y66 carbonyl oxygen atom of an enolate species containing a double bond between the Y66 carbonyl carbon atom and either a deprotonated G67 nitrogen or deprotonated Y66 Cα atom (Figure 5). Given typical pK_a values in peptides, G67 main chain nitrogen deprotonation would be favored over Y66 Cα deprotonation, yet both may occur at different steps in the reaction mechanism. Through water-mediated interactions, nearby conserved residue E222 could serve as a general base to favor either or both of these deprotonation reactions. Y66−G67 double bond formation coupled with G67 nitrogen deprotonation would facilitate peptide cyclization through nucleophilic attack of the G67 nitrogen lone pair on the S65 carbonyl carbon atom (*25*). Y66 Cα−C double bond formation coupled with Y66 Cα deprotonation after peptide cyclization and dehydration is proposed to generate an enolate intermediate (Figure 5) that may be critical for stabilizing the cyclized moiety and allowing chromophore maturation to proceed (*25*). Therefore, we propose that the functionally important electrostatic role of the R96 positive charge is to acidify the G67 backbone nitrogen and/or Y66 Cα atoms.

SUMMARY

Our results indicate a primarily electrostatic role for conserved R96 in the post-translational modification for this class of fluorescent protein. The positive electrostatic role of GFP R96 may have a functional equivalent [via helix dipoles (*12*)] in the similar peptide backbone cyclization reactions that create electrophile catalysts for the enzymes histidine ammonia lyase and phenylalanine ammonia lyase (*10*, *12*). In GFP, the loss of this positive charge at position 96 alters the rate-limiting step of chromophore maturation from oxidation (in wild-type GFP) to cyclization, suggesting that R96 has a functional role in forming and/or stabilizing the cyclized moiety. We favor a role for R96 in facilitating deprotonation of the G67 backbone nitrogen to promote ring formation. Future GFP studies may include coupling aerobic and anerobic maturation with structural studies for the R96M variant to test the role of R96 in stabilizing this cyclized intermediate prior to chromophore oxidation and probe the role of R96 in chromophore oxidation. In addition, the utilization of a similar slow-forming variant may allow isolation and characterization of additional maturation intermediates in GFP and its RFP homologues. Together, these studies provide an in-depth understanding of the architectural

driving force and assisting protein chemistry in this fascinating class of fluorescent proteins that is critical for the design and creation of novel chromophores with desirable photophysical properties.

NOTE ADDED IN PROOF

Our structural and biochemical analyses are further supported by recent complementary spectroscopic and biochemical studies on GFP variants by Wachter and colleagues (*41*, *42*). These investigators similarly assigned an electrophilic role for R96 in stabilizing an enolate intermediate, based on chromophore pK_a, maturation rate and spectral properties for the R96M and R96K variants. They also characterized the E222Q variant and provided evidence that E222 serves as a general base favoring deprotonation coupled to enolate formation, consistent with our analyses.

ACKNOWLEDGMENT

We thank Christopher D. Putnam and Joy L. Huffman for scientific discussions and critical reading of the manuscript. We also thank David S. Shin for help in labeling the stereo figures.

SUPPORTING INFORMATION AVAILABLE

Stereo model of the R96K variant within the context of the R96M precyclized backbone (Figure 1) and fluorescence phenotype assay results of the 20 R96 variants (Figure 2). This material is available free of charge via the Internet at http://pubs.acs.org.

REFERENCES

1. Cubitt, A. B., Woollenweber, L. A., and Heim, R. (1999) Understanding structure−function relationships in the *Aequorea victoria* green fluorescent protein, *Methods Cell Biol. 58*, 19−30.
2. Ormo, M., Cubitt, A. B., Kallio, K., Gross, L. A., Tsien, R. Y., and Remington, S. J. (1996) Crystal structure of the *Aequorea victoria* green fluorescent protein, *Science 273*, 1392−5.
3. Heim, R., Prasher, D. C., and Tsien, R. Y. (1994) Wavelength mutations and posttranslational autoxidation of green fluorescent protein, *Proc. Natl. Acad. Sci. U.S.A. 91*, 12501−4.
4. Yang, F., Moss, L. G., and Phillips, G. N., Jr. (1996) The molecular structure of green fluorescent protein, *Nat. Biotechnol. 14*, 1246−51.
5. Robey, R. B., Ruiz, O., Santos, A. V., Ma, J., Kear, F., Wang, L. J., Li, C. J., Bernardo, A. A., and Arruda, J. A. (1998) pH-dependent fluorescence of a heterologously expressed *Aequorea* green fluorescent protein mutant: In situ spectral characteristics and applicability to intracellular pH estimation, *Biochemistry 37*, 9894−901.
6. Kneen, M., Farinas, J., Li, Y., and Verkman, A. S. (1998) Green fluorescent protein as a noninvasive intracellular pH indicator, *Biophys. J. 74*, 1591−9.
7. Kain, S. R., Adams, M., Kondepudi, A., Yang, T. T., Ward, W. W., and Kitts, P. (1995) Green fluorescent protein as a reporter of gene expression and protein localization, *BioTechniques 19*, 650−5.
8. Barondeau, D. P., Kassmann, C. J., Tainer, J. A., and Getzoff, E. D. (2002) Structural chemistry of a green fluorescent protein Zn biosensor, *J. Am. Chem. Soc. 124*, 3522−4.
9. Elsliger, M. A., Wachter, R. M., Hanson, G. T., Kallio, K., and Remington, S. J. (1999) Structural and spectral response of green fluorescent protein variants to changes in pH, *Biochemistry 38*, 5296−301.
10. Schwede, T. F., Retey, J., and Schulz, G. E. (1999) Crystal structure of histidine ammonia-lyase revealing a novel polypeptide modification as the catalytic electrophile, *Biochemistry 38*, 5355−61.
11. Poppe, L. (2001) Methylidene-imidazolone: A novel electrophile for substrate activation, *Curr. Opin. Chem. Biol. 5*, 512−24.
12. Calabrese, J. C., Jordan, D. B., Boodhoo, A., Sariaslani, S., and Vannelli, T. (2004) Crystal structure of phenylalanine ammonia lyase: Multiple helix dipoles implicated in catalysis, *Biochemistry 43*, 11403−16.
13. Wiehler, J., von Hummel, J., and Steipe, B. (2001) Mutants of *Discosoma* red fluorescent protein with a GFP-like chromophore, *FEBS Lett. 487*, 384−9.
14. Gross, L. A., Baird, G. S., Hoffman, R. C., Baldridge, K. K., and Tsien, R. Y. (2000) The structure of the chromophore within DsRed, a red fluorescent protein from coral, *Proc. Natl. Acad. Sci. U.S.A. 97*, 11990−5.
15. Petersen, J., Wilmann, P. G., Beddoe, T., Oakley, A. J., Devenish, R. J., Prescott, M., and Rossjohn, J. (2003) The 2.0-Å crystal structure of eqFP611, a far red fluorescent protein from the sea anemone *Entacmaea quadricolor*, *J. Biol. Chem. 278*, 44626−31.
16. Mizuno, H., Mal, T. K., Tong, K. I., Ando, R., Furuta, T., Ikura, M., and Miyawaki, A. (2003) Photoinduced peptide cleavage in the green-to-red conversion of a fluorescent protein, *Mol. Cell 12*, 1051−8.
17. Zagranichny, V. E., Rudenko, N. V., Gorokhovatsky, A. Y., Zakharov, M. V., Balashova, T. A., and Arseniev, A. S. (2004) Traditional GFP-type cyclization and unexpected fragmentation site in a purple chromoprotein from *Anemonia sulcata*, asFP595, *Biochemistry 43*, 13598−603.
18. Shaner, N. C., Campbell, R. E., Steinbach, P. A., Giepmans, B. N., Palmer, A. E., and Tsien, R. Y. (2004) Improved monomeric red, orange and yellow fluorescent proteins derived from *Discosoma* sp. red fluorescent protein, *Nat. Biotechnol. 22*, 1567−72.
19. Zhang, J., Campbell, R. E., Ting, A. Y., and Tsien, R. Y. (2002) Creating new fluorescent probes for cell biology, *Nat. Rev. Mol. Cell Biol. 3*, 906−18.
20. Reichel, C., Mathur, J., Eckes, P., Langenkemper, K., Koncz, C., Schell, J., Reiss, B., and Maas, C. (1996) Enhanced green fluorescence by the expression of an *Aequorea victoria* green fluorescent protein mutant in mono- and dicotyledonous plant cells, *Proc. Natl. Acad. Sci. U.S.A. 93*, 5888−93.
21. Wachter, R. M., Elsliger, M. A., Kallio, K., Hanson, G. T., and Remington, S. J. (1998) Structural basis of spectral shifts in the yellow-emission variants of green fluorescent protein, *Structure 6*, 1267−77.
22. Barondeau, D. P., Putnam, C. D., Kassmann, C. J., Tainer, J. A., and Getzoff, E. D. (2003) Mechanism and energetics of green fluorescent protein chromophore synthesis revealed by trapped intermediate structures, *Proc. Natl. Acad. Sci. U.S.A. 100*, 12111−6.
23. Branchini, B. R., Nemser, A. R., and Zimmer, M. (1998) A computational analysis of the unique protein induced tight turn that results in posttranslational chromophore formation in green fluorescent protein, *J. Am. Chem. Soc. 120*, 1−6.
24. Heim, R., Cubitt, A. B., and Tsien, R. Y. (1995) Improved green fluorescence, *Nature 373*, 663−4.
25. Barondeau, D. P., Kassmann, C. J., Tainer, J. A., and Getzoff, E. D. (2005) Understanding GFP Chromophore Biosynthesis: Controlling Backbone Cyclization and Modifying Post-translational Chemistry, *Biochemistry 44*, 1960−70.
26. Reid, B. G., and Flynn, G. C. (1997) Chromophore formation in green fluorescent protein, *Biochemistry 36*, 6786−91.
27. Deschamps, J. R., Miller, C. E., and Ward, K. B. (1995) Rapid purification of recombinant green fluorescent protein using the hydrophobic properties of an HPLC size-exclusion column, *Protein Expression Purif. 6*, 555−8.
28. Otwinowski, Z., and Minor, W. (1997) Processing of X-ray Diffraction Data Collected in Oscillation Mode, *Methods Enzymol. 276*, 307−26.
29. Collaborative Computational Project, No. 4 (1994) The CCP4 Suite: Programs for Protein Crystallography, *Acta Crystallogr. D50*, 760−3.
30. McRee, D. E. (1999) XtalView/Xfit: A versatile program for manipulating atomic coordinates and electron density, *J. Struct. Biol. 125*, 156−65.
31. Brunger, A. T., Adams, P. D., Clore, G. M., DeLano, W. L., Gros, P., Grosse-Kunstleve, R. W., Jiang, J. S., Kuszewski, J., Nilges, M., Pannu, N. S., Read, R. J., Rice, L. M., Simonson, T., and Warren, G. L. (1998) Crystallography & NMR system: A new software suite for macromolecular structure determination, *Acta Crystallogr. D54* (Part 5), 905−21.
32. Sheldrick, G. M., and Schneider, T. R. (1997) SHELXL: High-resolution refinement, *Methods Enzymol. 277*, 319−43.
33. Craig Upson, T. F., Jr., Kamins, D., Laidlaw, D., Schlegel, D., Vroom, J., Gurwitz, R., and van Dam, A. (1989) The Application

Visualization System: A Computational Environment for Scientific Visualization, *IEEE Comput. Graphics Appl. 9*, 30−42.
34. Crameri, A., Whitehorn, E. A., Tate, E., and Stemmer, W. P. (1996) Improved green fluorescent protein by molecular evolution using DNA shuffling, *Nat. Biotechnol. 14*, 315−9.
35. Cormack, B. P., Valdivia, R. H., and Falkow, S. (1996) FACS-optimized mutants of the green fluorescentprotein (GFP), *Gene 173*, 33−8.
36. Tsien, R. Y. (1998) The green fluorescent protein, *Annu. Rev. Biochem. 67*, 509−44.
37. Heim, R., and Tsien, R. Y. (1996) Engineering green fluorescent protein for improved brightness, longer wavelengths and fluorescence resonance energy transfer, *Curr. Biol. 6*, 178−82.
38. Wachter, R. M., Yarbrough, D., Kallio, K., and Remington, S. J. (2000) Crystallographic and energetic analysis of binding of selected anions to the yellow variants of green fluorescent protein, *J. Mol. Biol. 301*, 157−71.
39. Siegbahn, P. E. M., Wirstam, M., and Zimmer, M. (2001) Theoretical study of the mechanism of peptide ring formation in green fluorescent protein, *Int. J. Quantum Chem. 81*, 169−86.
40. Goto, Y., and Klinman, J. P. (2002) Binding of dioxygen to non-metal sites in proteins: Exploration of the importance of binding site size versus hydrophobicity in the copper amine oxidase from *Hansenula polymorpha*, *Biochemistry 41*, 13637−43.
41. Sniegowski, J. A., Phail, M. E., and Wachter, R. M. (2005) Maturation efficiency, trypsin sensitivity, and optical properties of Arg96, Glu222, and Gly67 variants of green fluorescent protein, *Biochem. Biophys. Res. Commun. 332*, 657−63.
42. Sniegowski, J. A., Lappe, J. W., Patel, H. N., Huffman, H. A., and Wachter, R. M. (2005) Base catalysis of chromophore formation in Arg96 and Glu222 variants of green fluorescent protein, *J. Biol. Chem. 280*, 26248−55.

BI051388J